International Journal of Refractory Metals and Hard Materials 117 (2023) 106375

Contents lists available at ScienceDirect

International Journal of Refractory Metals and Hard Materials

journal homepage: www.elsevier.com/locate/IJRMHM

WC-Ni cemented carbides prepared from Ni nano-dot coated powders

Paul H. Gruber [a], Sarmad Naim Katea [b], Gunnar Westin [b,*], Farid Akhtar [a,*]

[a] Department of Engineering Sciences and Mathematics, Materials Science, Luleå University of Technology, 971 87 Luleå, Sweden
[b] Department of Chemistry - Ångström Laboratory, Uppsala University, 751 21 Uppsala, Sweden

ARTICLE INFO

Keywords:
Cemented carbides
Coated powders
WC-Ni
Sinterability
Solution processing
Mechanical properties

ABSTRACT

This study presents a novel approach for the synthesis of WC-Ni cemented carbides with enhanced mechanical properties. A low-cost solution-based route was used to coat WC powders with well-distributed metallic nickel dots measuring between 17 nm and 39 nm in diameter. Varying compositions with loadings of 2, 6, and 14 vol% Ni were consolidated using spark plasma sintering (SPS) at 1350 °C under 50 MPa of uniaxial pressure giving relative densities of 99 ± 1 %. The sintered WC-Ni cemented carbides had an even distribution of the Ni binder phase in all compositions, with retained ultrafine WC grain sizes of 0.5 ± 0.1 μm from the starting powder. The enhanced sinterability of the coated powders allowed for consolidation to near theoretical densities, with a binder content as low as 2 vol%. This is attributed to the uniform distribution of nickel and an extensive Ni-WC interface existing prior to sintering. The small size of the Ni dots likely also contributed to the solid-state sintering starting temperatures of as low as 800 °C. The mechanical performance of the resulting cemented carbides was evaluated by measuring the hardness at temperatures between 20 °C and 700 °C and estimating toughness at room temperature using Vickers indentations. These results showed that the mechanical properties of the WC-Ni cemented carbides synthesised by our method were comparable to conventionally prepared WC-Co cemented carbides with similar grain sizes and binder contents and superior to conventionally prepared WC-Ni cemented carbides. In particular, the 2 vol% Ni composition had excellent hardness at room temperature of up to 2210HV10, while still having an indentation fracture toughness of 7 MPa·m$^{0.5}$. Therefore, WC-Ni cemented carbides processed by this novel approach are a promising alternative to conventional WC-Co cemented carbides for a wide range of applications.

1. Introduction

Finding alternatives to the conventionally used cobalt binders in WC-based cemented carbides has been an ongoing endeavour for decades due to the depletion of resources, geopolitical reasons, its toxicity, greater demands on corrosion resistance, or when a non-magnetic character is required. Nickel is one of the most promising substitutes for cobalt, with WC-Ni cemented carbides being researched for nearly a century after their invention in 1923 by Schröter [1]. The lower cost, higher corrosion resistance [2], non-magnetic behaviour [3,4], and higher fracture toughness [5] of Ni compared to Co make it an attractive binder for applications in corrosive environments and other special applications. However, studies on first-generation WC-Ni cemented carbides found inferior mechanical properties, such as lower hardness and transverse rupture strength, compared to WC-Co [2,5–7]. The low wettability of Ni on WC surfaces and lower solubility of WC in Ni [5] have been reported to reduce the sinterability and mechanical properties of the sintered cemented carbides.

Several modifications to materials and process variables may be considered to enhance the sinterability and thereby improve the mechanical properties of cemented carbides, with particle size and mixedness of the constituent powders being the most influential [8]. Suzuki et al. [9] reported similar mechanical properties in Co- and Ni-based cemented carbides when the WC grain size was reduced to 0.4 μm. Similar results were reported for WC grain sizes of 0.3 μm utilising mechanical milling prior to sintering [10,11] exhibiting the true potential of WC-Ni when material and/or process variables are optimised. Powder coating is another effective way to improve the sinterability of WC powders, whereby Ni is deposited on the surface of WC particles. This establishes a good distribution and large contact area between WC and Ni, compared to conventional powder mixing of the two constituents. The coating also ensures a sustained distribution of the constituents

* Corresponding author.
E-mail addresses: paul.gruber@ltu.se (P.H. Gruber), sarmad.katea@kemi.uu.se (S. Naim Katea), Gunnar.Westin@kemi.uu.se (G. Westin), farid.akhtar@ltu.se (F. Akhtar).

https://doi.org/10.1016/j.ijrmhm.2023.106375
Received 21 June 2023; Received in revised form 17 August 2023; Accepted 18 August 2023
Available online 24 August 2023

and reduces the risk of the presence of oxide barrier layers between Ni and WC. Researchers have developed simple, salt-based solution routes to coat different carbides and other ceramics with metallic Ni, Fe, and Co in the form of dense layers or well-distributed nano-dots [12–16]. Cemented carbides prepared from such coated powders are particularly interesting as the powders exhibited enhanced sinterability and yielded better control over the resulting microstructure compared to powder mixtures. The well-adhered coatings provided a large area of direct contact between metal and carbide, ensured good distribution of the binder metal, and provided short diffusion paths. The use of low-cost equipment and readily available chemicals make this method highly scalable compared to more laborious powder preparation methods such as sputtering [17] or processing using unique chemicals [18].

Sintering parameters such as temperature, heating rate, applied pressure, and atmosphere during consolidation can be altered as well to enhance sinterability. Spark Plasma Sintering (SPS) has proven to be a reliable sintering method to produce cemented carbides of high density with little to no grain-growth and excellent mechanical properties [19,20]. It provides greater control over microstructural development compared to conventional methods.

In this work, a novel processing route for WC-Ni cemented carbides using Ni nano-dot coated powders and SPS was evaluated. Ultrafine submicrometre WC powders were coated with Ni using the solution-based technique developed by Ekstrand et al. [14,15]. Sintering behaviour and microstructural evolution during SPS were investigated. The Ni-dot coating is expected to increase sinterability significantly, thereby allowing for the realisation of cemented carbides with extremely low binder phase fractions. Nickel contents of 2, 6, and 14 vol% were chosen to investigate a wide range of binder contents from typical cutting tool compositions, containing 14 vol% Ni, down to almost binder-less compositions of only 2 vol% Ni. The resulting cemented carbides were analysed using SEM, EDS, and XRD. The mechanical performance was assessed by measuring hardness from room temperature up to 700 °C and estimating room temperature toughness using the Vickers indentation crack length method. The results were compared to literature published on WC-Ni and WC-Co cemented carbides processed by conventional and non-conventional methods.

2. Material and methods

2.1. Starting materials

Nickel (II) nitrate hexahydrate ($Ni(NO_3)_2{\cdot}6H_2O$, Sigma-Aldrich), nickel (II) acetate tetrahydrate ($Ni(OAc)_2{\cdot}4H_2O$ > 98 %, Sigma-Aldrich), methanol (analytical grade 99.9% Scharlau), triethanolamine (TEA, ≥ 99 %, Sigma Aldrich), and tungsten carbide (WC, D.S. 60, H.C. Starck Tungsten GmbH) were used as received. According to the manufacturer's data sheet, the WC powder contained 6.11 wt% total C and 0.02 wt% free carbon and had a Fisher particle size of 0.64 μm. More details of the chemical analysis of the WC powder are given in the supplementary information Table S1. Furthermore, a few abnormally large WC particles within the otherwise homogeneous powder of somewhat agglomerated WC particles were found, as shown in Fig. S2 in the supplementary information.

2.2. Powder coating

The WC-Ni powders coated with 2, 6, and 14 vol% Ni were prepared as follows: A methanolic nickel precursor solution with a nitrate:acetate ratio of 9:1 and 0.5 triethanolamine (TEA) per nickel was made according to previous work [15,16]. Then, the nickel precursor solution was added to the WC powder in amounts yielding 2, 6, and 14 vol% Ni [13]. After evaporation of the methanol, the obtained dough-like mixture was heated under an Ar atmosphere (Ar gas N57, purity > 99.9997 %) at 10 °C/min to 500 °C. The 14 vol% Ni powder was prepared by two coating cycles of 7 vol% Ni, each with heating to 500 °C at 10 °C/min in an Ar gas atmosphere. The heat treatments were made in a split tube furnace on porous powder beds in a boat made of stainless steel with an Argon gas flow rate of 200 mL/min. The silica tube was sealed at each end by a steel plate with Leybold couplings and gas-pipe throughputs [13].

2.3. Sintering

The nickel dot-coated powder was consolidated using SPS (Dr. Sinter 2050, Sumitomo Coal Mining Co.). The powders were poured into 10 mm diameter graphite dies with graphite sheet lining. A uniaxial pressure of 50 MPa was applied during the heating and holding cycle. A heating rate of 100 °C/min was used during heating from room temperature up to 600 °C, where the specimens were held for 1 min. Next, the specimens were heated up to 1350 °C, using a heating rate of 100 °C/min, and were held there for 2 min. Subsequently, the heating was turned off, and the pressure was released once the temperature dropped below 1000 °C. The specimens were left to cool in the SPS to around 100 °C before removal. The atmosphere was air at 10 to 30 Pa pressure during the sintering cycle. Two specimens were produced from each composition, one for microstructural analysis (MS), and one for high-temperature mechanical testing (HT), resulting in a total of 6 specimens. After sintering, the surface of the specimen was ground using 220 grit SiC paper to remove adhering graphite from the SPS die lining.

2.4. Microstructural analysis

The Ni-coated WC powders were studied with a Merlin Scanning Electron Microscope (SEM, Zeiss) equipped with an Energy Dispersive Spectrometer (EDS). The microstructural analysis of sintered WC-Ni specimens (MS) was made on axially cut cross-sections using a Magellan 400 Extreme-High Resolution SEM, (FEI Company) equipped with an EDS. The crystallinity of the Ni dot-coated WC powders and cut MS specimens was studied by X-ray diffraction in θ-2θ mode (XRD, Empyrean, Malvern Panalytical) using Cu-Kα radiation with 40 kV and 40 mA, a step size of 0.013 ° and 60 s dwell time. Light optical microscopy (LOM) was used to image the total cross-section of the MS specimens. A second set of sintered WC-Ni specimens (HT) were cut parallel with 1–2 mm offset from the cylinder faces. The larger slices were used for the HT testing and were also analysed with SEM and XRD. Density measurements were performed using Archimedes' principle on MS and HT specimens. Grain size was estimated from SEM images of the MS specimens using the linear intercept method according to literature [21]. For each reported grain size two images containing 5 lines each at 33000 times magnification were analysed.

2.5. Mechanical properties

An in-house built hardness tester with low vacuum capability was used for high temperature (HT) hardness tests as described elsewhere [22]. The hardness was calculated from Vickers' indentations made with a 10 kg load and 13 s holding time using the equation

$$HV = 0.1891\frac{F}{\left(\frac{D_v+D_h}{2}\right)^2}$$

where F is the load in N and D_v, and D_h are the indent's diagonal lengths in mm (shown in Fig. 1). Three indentations were made for each reported hardness value. The atmosphere during indentation was air at <500 Pa. Temperatures were increased from room temperature to 100 °C and then in 100 °C steps up to 700 °C, as shown in Fig. 2. The indentations were measured in two cycles after indentation at 400 and 700 °C, after cooling the specimens to room temperature in a separate optical microscope. An additional sixteen indentations were made for each composition after the HT test using a regular hardness tester (Duramin-40, Struers) using the same load and equation. Fracture

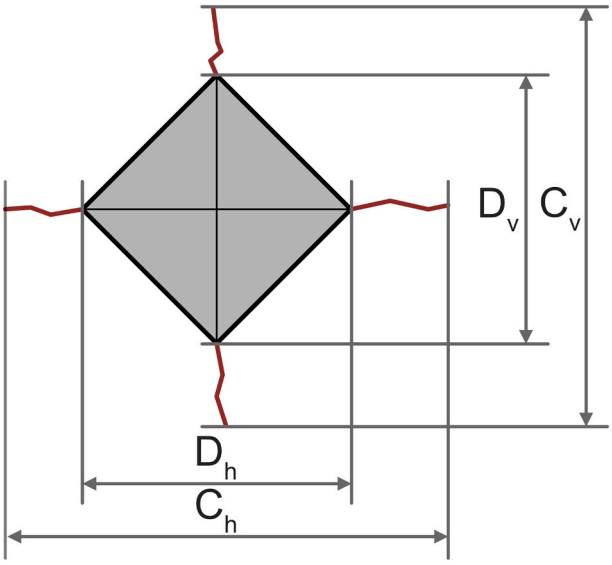

Fig. 1. Schematic diagram of a Vickers' indent showing the indented area and the resulting cracks visible on the surface.

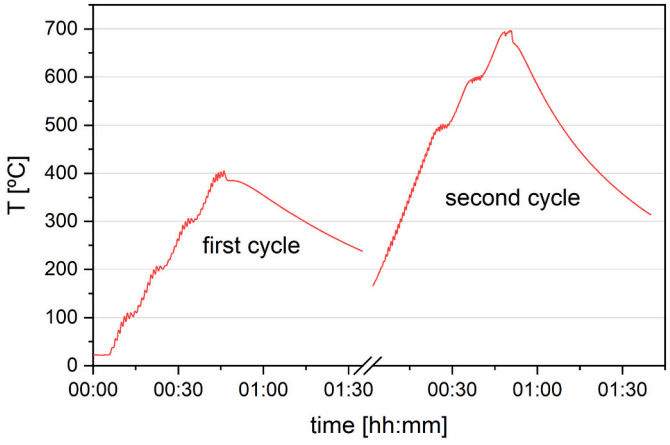

Fig. 2. Thermal history during high-temperature testing.

toughness K_{IC} was estimated from these additional indentations by the commonly used Palmquist fracture toughness Eq. [23].

$$K_{IC} \approx W_K = 0.0028\sqrt{HV \cdot 9.81}\sqrt{\frac{F}{C_v - D_v + C_h - D_h}}$$

where W_k is the indentation fracture toughness, HV is the Vickers hardness number, F is the load in N, D_v and D_h are the indent's diagonal lengths in mm, and C_v and C_h are the vertical and horizontal distances between the crack tips in mm (shown in Fig. 1).

3. Results and discussion

3.1. Nickel coated WC powders

The SEM micrographs of the initial WC powder and Ni-dot coated WC powders given in Fig. 3, show that the Ni dots were evenly distributed over the WC particle surfaces. The Ni-dot size and coverage increased with Ni loading. The number average Ni dot sizes measured from the dots visible in the SEM images were 17, 24, and 39 nm for WC2Ni, WC6Ni, and WC14Ni power, respectively. This is comparable to the 5 to 30 nm sized Ni dots Naim Katea et al. [13] obtained on NbC powder with 3.5 to 12.5 vol% Ni loading using the same coating routine. Additional SEM micrographs of the powders are available in the supplementary information.

The X-ray diffractograms of the initial WC powder and coated powders are presented in Fig. 4. The deposition of Ni nano-dots on the WC powder particles did not alter the WC peak positions or width, showing that no significant crystallographic or compositional changes in the carbide particles occurred due to the coating process. The fcc Ni (111) and Ni (200) peaks for WC6Ni and WC14Ni powders show that the deposited Ni nano-dots were crystalline. The lattice parameter of the Ni dots was determined for WC6Ni and WC14Ni, using the (111) peak of fcc Ni (Table 1). The obtained value of 3.54 Å was slightly larger than the reference value of 3.523 Å (PDF 04–010-6148). This can be the result of the epitaxial growth of Ni on the WC surface [13], a marginal uptake of C [24] and/or W [25], and the small sizes of the crystallites. The Ni peaks in WC2Ni were not detected, which is ascribed to the small crystallite size in combination with the lower volume fraction of Ni compared to the higher Ni loadings [25].

3.2. Consolidation

During consolidation in the SPS, the die displacement was recorded and is shown in Fig. 5, together with the calculated die displacement rate (DDR). The die displacement (DD) curves are normalised for identical total displacements. Individual curves for all specimens can be found in the supplementary information in Fig. S3. The thermal expansion of the SPS punches and electrodes was not corrected, and therefore, the die displacement is the sum of the shrinkage due to sintering and the thermal expansion due to temperature change.

The consolidation happened in two distinct stages, as shown in Fig. 5. Below 800 °C, the DDRs remained relatively low as only little compaction occurred, presumably originating from the rearrangement of particles and plastic deformation of Ni dots due to the applied pressure and increasing temperature. However, some compaction due to reactions between the Ni dots and WC cannot be excluded. In nanocrystalline pure Co and Ni sponges synthesised in a similar way, rapid crystal growth was observed at 450 °C, which shows that the nanocrystals were quite active even at these low temperatures [16]. Melting point depression is also known for small nano-particles where drastically reduced melting points can be observed compared to bulk specimens [26]. Higher Ni loadings resulted in higher DDRs in the early stage due to lower bulk densities obtained from the rougher powder particles. At higher temperatures, the DDRs increased rapidly due to the beginning of the sintering. The general sintering start temperatures were between 800 °C and 900 °C, and the greatest DDRs were found around 1135 °C, while with higher Ni contents, a tendency toward earlier sintering was shown, as well as lower temperature at their greatest DDR. The sintering start temperatures were below Ni's melting point or any Ni-W solid solution [27]. No further consolidation took place during the 2 min hold at 1350 °C. Furthermore, localised elevated temperatures during SPS could have caused the Ni dots to melt at the observed temperatures [20].

For cemented carbides, Macedo et al. [28] described that Ni can spread already at 800 °C on carbide surfaces and described the spreading as a material flow based on the diffusion of atoms in the highly disordered and defect-rich interface layer between binder metal and carbide. They also found that high heating rates are necessary to keep the interface layer from ordering, thereby impairing material flow.

It is not clear whether liquid phase sintering takes place after the sintering start temperature or whether it is diffusion based solid-state sintering. Due to melting point depression and localised heating, a liquid phase likely formed before reaching 1350 °C facilitating the final densification.

The density measurements of the consolidated specimens are shown in Fig. 6. A significant deviation in relative density of > 1 % between MS and HT specimens was evident for WC2Ni and WC14Ni. However, a trend was seen that higher Ni contents resulted in higher relative

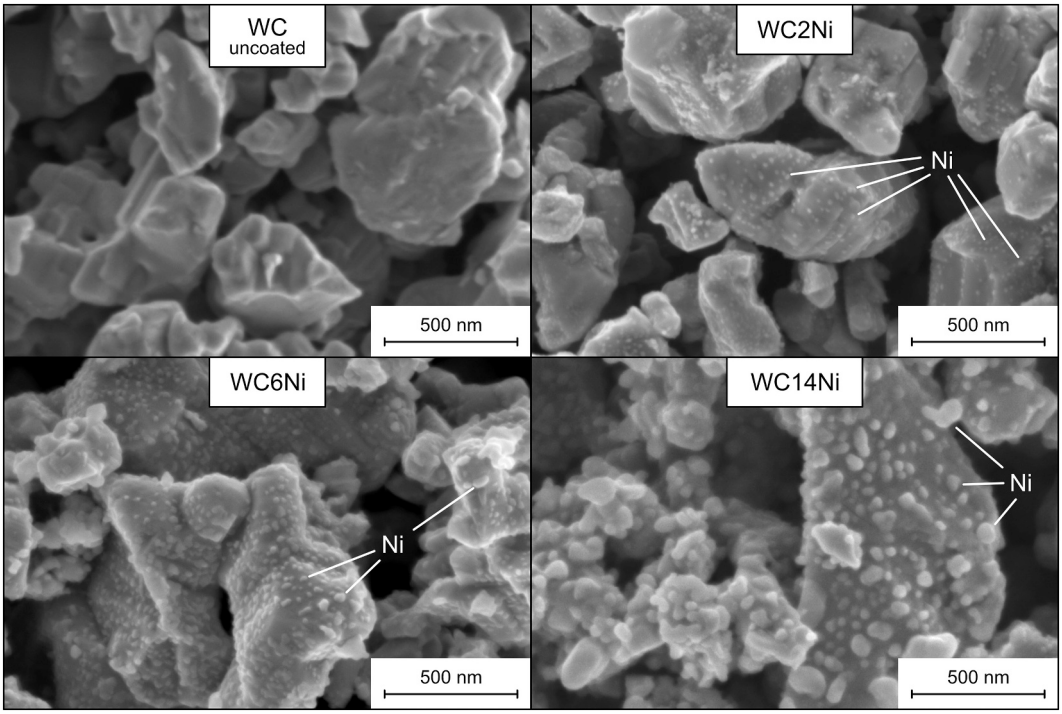

Fig. 3. SEM micrographs of Ni-dot coated WC powders after heating to 500 °C using an in-lens detector. The particles lighter in appearance are the Ni dots.

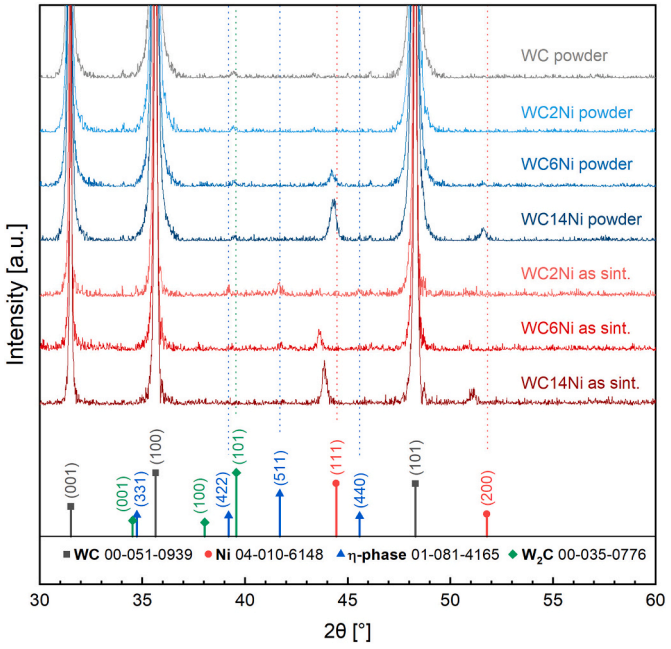

Fig. 4. XRD diffractograms of the initial WC powder, coated powders, and the consolidated specimens.

densities. The average relative density was 0.99 ± 0.01. The theoretical density was calculated using the nominal values of Ni loading.

Cross-sections after consolidation in Fig. 7 taken with LOM show a darker region near the surface of the specimens. EDX line scans revealed a reduced Ni content in this casing region that was separated by a narrow high Ni zone from the homogeneous core of the specimen. The depth of this separation zone was 0.5 ± 0.1 mm from the surface.

The Ni redistribution close to the surface during SPS has yet to be fully understood. It could be related to the carbon sheet lining used in the SPS die that potentially carburized the material from the outside. In WC-Co composites, similar macro-gradients are produced by deliberately carburising the outer layer of parts [29,30]. The following binder redistribution during liquid phase sintering produces comparable depleted casing and enriched separation zones.

Table 1
Peak position, interplanar spacing, lattice parameter, and peak width from XRD analysis of the fcc Ni (111) peak compared to the database PDF.

Composition	State	2θ [°]	$d_{Ni(111)}$ [Å]	a [Å]	FWHM [°]
WC6Ni	powder	44.229 ± 0.010	2.0462	3.5441	0.27
	as sintered	43.623 ± 0.010	2.0732	3.5908	0.20
WC14Ni	powder	44.286 ± 0.005	2.0437	3.5397	0.35
	as sintered	43.867 ± 0.008	2.0622	3.5719	0.25
fcc-Ni 04–010-6148	powder	44.433		3.523	

Some material escaped through a gap in the graphite sheet lining during SPS of the MS specimen WC14Ni and was visible on the outside of the die after SPS as a small drop. This most likely explains the relative density of over 100 % as the liquid phase must have been composed mostly of Ni and therefore alters the chemical composition slightly, underestimating the theoretical density. The drop also further attests to the formation of a liquid phase during SPS despite sintering below the melting point of Ni.

Considering the short SPS time and high relative densities, the dot-coated powders exhibited great sinterability despite their relatively low Ni concentrations, especially for WC2Ni. A temperature of 1350 °C was satisfactory for achieving highly dense specimens, which agrees with the findings by Lima et al. [18] where a temperature of 1350 °C gave the best results for WC-Ni when using SPS. High heating rates were used to facilitate the Ni-dots spreading over the carbide's surface and by that solid-state sintering, as suggested by Macedo et al. [28]. However,

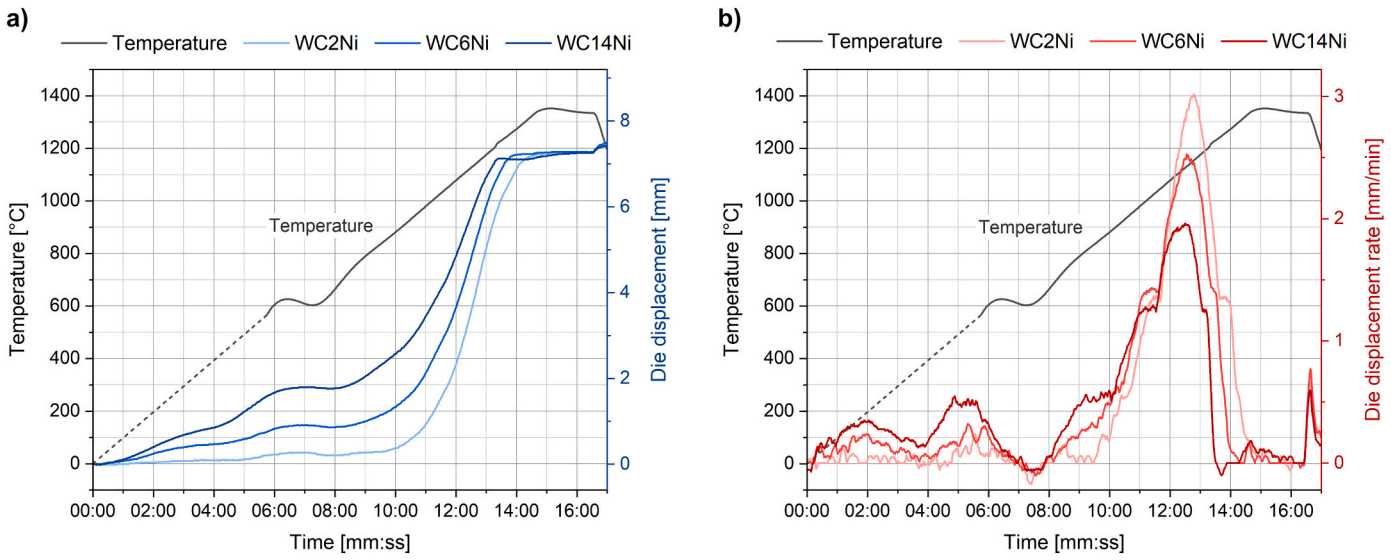

Fig. 5. a) Die Displacement (DD), b) Die Displacement Rate (DDR), and temperature during the SPS heating cycle.

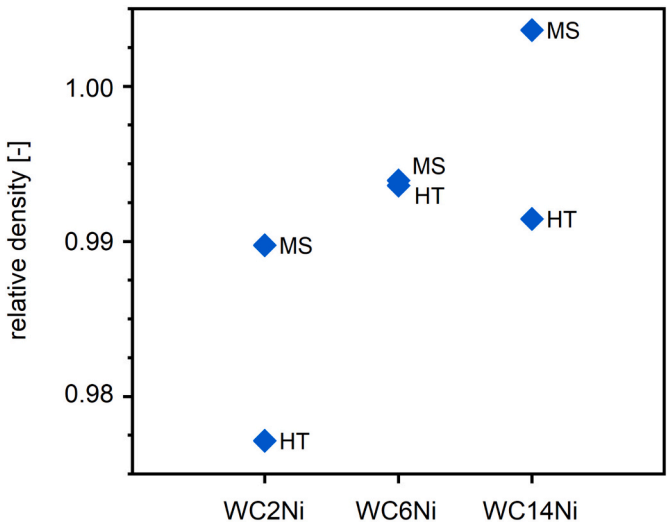

Fig. 6. Comparison of relative densities of consolidated specimens for the separately sintered MS (microstructural analysis) and HT (high temperature hardness testing) specimens.

the holding time of 2 min might not have been necessary, and shortening it could have reduced the amount of Ni redistribution.

3.3. Microstructure

Cross-sections of the consolidated specimen at two different magnifications are presented in Fig. 8. Prismatic WC particles of light to medium dark grey shades can be seen surrounded by the almost black Ni binder phase. All three compositions exhibit a similar average WC grain size of about 0.5 ± 0.1 µm. The WC grains in WC2Ni are conformed to each other, whereas grains that are prismatic and fairly well separated by binder phase can be seen in WC14Ni, while WC6Ni exhibits both features.

The XRD diffractograms of the powders and the consolidated MS specimens given in Fig. 4 show the presence of four phases: *hex* WC (00–051-0939), *fcc* Ni (04–010-6148), W_2C (00–035-0776), and η-phase (01–081-4165). The W_2C was absent from the diffractograms after SPS. However, traces of η-phase (e.g., W_4Ni_2C, PDF 01–081-4165) were detected in WC2Ni and WC6Ni after SPS, with a larger amount being present in WC2Ni. Quantitative data about the W_2C and η-phase could not be derived due to the minute amounts and few detectable peaks. The Ni peaks shifted even further to larger lattice parameters after SPS than the coated powders, especially for WC6Ni. The Ni phase could not be detected with XRD after SPS, similar to the Ni-coated WC2Ni powder. The lattice parameters and FWHM values derived from the Ni (111) peak are shown in Table 1. These data show that the Ni lattice parameter increased for WC6Ni and WC14Ni from powder to the sintered condition, whereas the FWHM value decreased. The expanded lattice of the Ni phase was most likely a result of uptake of C and W. Juskenas et al. [31]

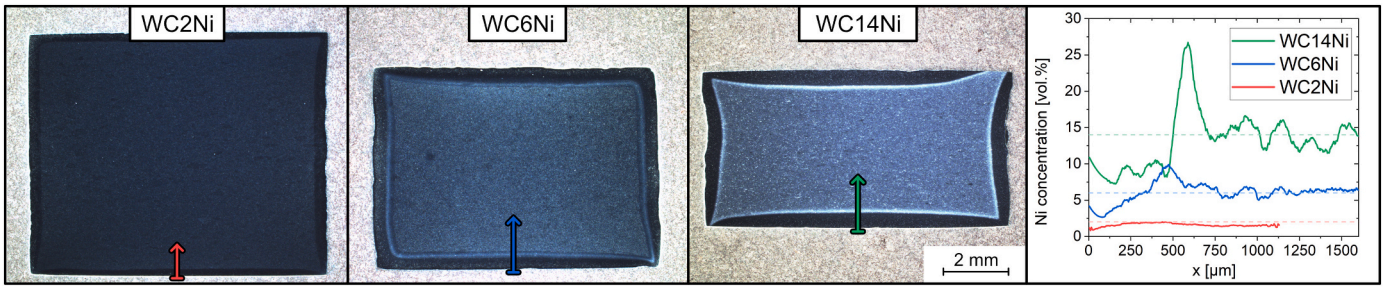

Fig. 7. Polished cross-section images taken with LOM and SEM-EDX line scan profiles; the specimens' cylinder axis is vertically oriented. The arrows indicate the range of the EDX line scans. The scale bar is valid for all three images.

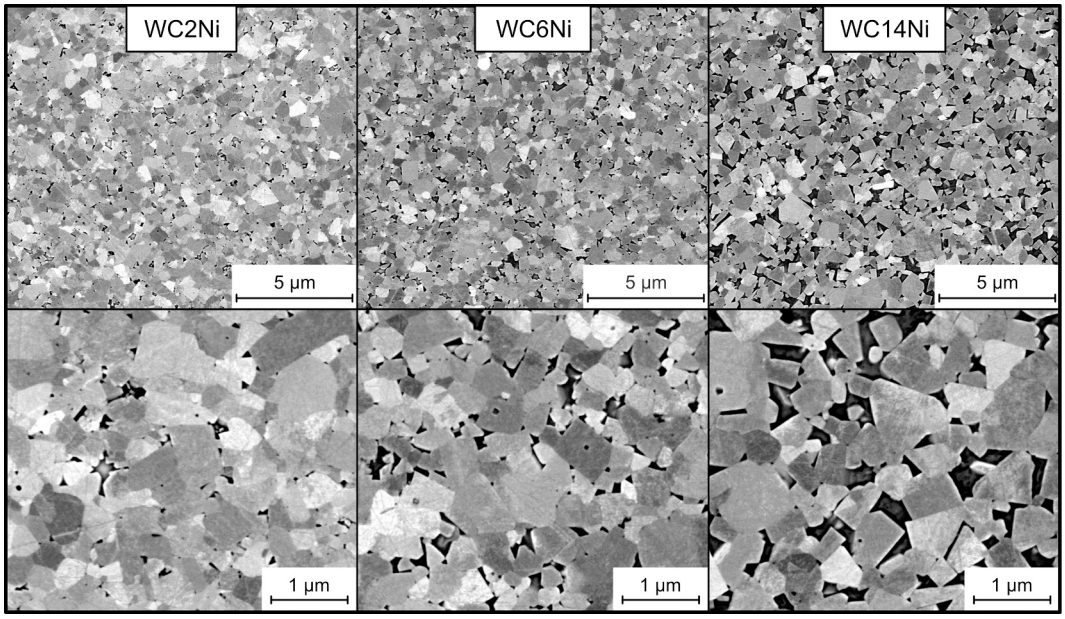

Fig. 8. SEM-BSE images showing the microstructures of the sintered specimens.

derived an expression to estimate the amount of W in a Ni-W solid solution from its lattice parameter a: $X_w = -7.5208 + 2.13429 * a$. Using this equation, the binder phase in WC14Ni and WC6Ni could consist of a Ni-W solid solution containing 10.3 at% and 14.3 at% W respectively. This estimation only considers the substitutionally dissolved W and ignores lattice expansion and a shift in the peak position caused by other factors, such as strains or interstitial atoms.

Together with the grain shape conformation of the carbide grains that require material transport, it can be concluded that the binder phase facilitated material transport for sintering. The obtained WC grain size of 0.5 ± 0.1 µm was independent of the Ni content and comparable to the initial powder grain size of 0.64 µm (Fischer number) of the initial WC powder. Therefore, no significant grain growth took place from the initial powders to the carbide grains.

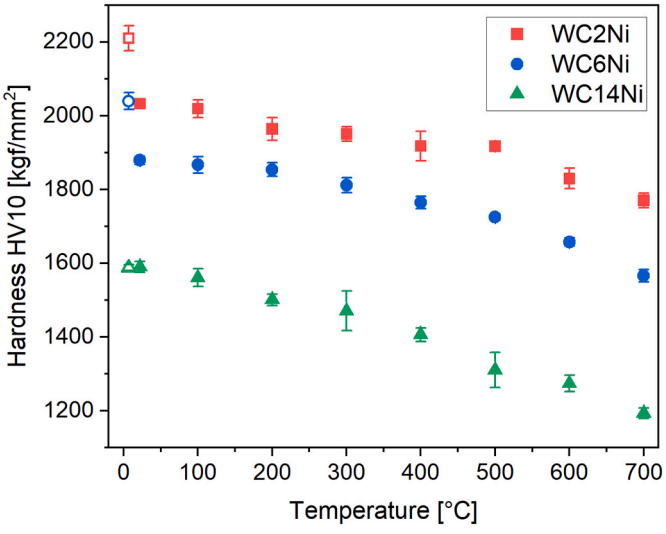

Fig. 9. HV10 hardness measurements at elevated temperatures. Hollow symbols show the second set of measurements at room temperature, after hardness testing at elevated temperature.

3.4. Hardness evaluation

The average hardness values obtained from HV10 Vickers indentations between room temperature and 700 °C are presented in Fig. 9, with absolute errors shown as error bars. All samples exhibited a gradual decrease in hardness with temperature without any abrupt changes. A second set of indentations was made at room temperature after the measurements up to 700 °C to assess whether the temperature cycle altered the room temperature properties, represented as hollow symbols in Fig. 9 and shown in Table 2, with error bars indicating the standard deviation. The RT hardness for WC2Ni and WC6Ni increased after testing, contrary to WC14Ni, where no change was observed. XRD diffractograms of the HT specimens after the measurements up to 700 °C exhibited no significant alterations in crystallography compared to the MS specimens. The increase in hardness may be attributed to the presence of small amounts of η-phase in these compositions, but no further investigations were conducted in this regard.

A comparison between room temperature hardness (after HT testing) and literature values is shown in Fig. 10. As the WC grain size substantially impacts hardness [29], the respective values are indicated for all data. With a hardness of 1588 HV, WC14Ni is on par with WC-Ni cemented carbides with similar binder fractions and grain sizes. It exhibits a comparable decrease in hardness of 100 to 200 HV compared to WC-Co, as suggested in Tracey's work [5]. On the other hand, WC2Ni and WC6Ni demonstrated significantly higher hardness than any other WC-Ni compositions with similar grain sizes reported in the literature, as shown in Fig. 10. Their values are comparable to WC-Ni cemented carbides with grain sizes of 0.024 µm [18], which is 20 times smaller. WC2Ni demonstrated an impressive hardness of 2210 HV, which approaches the upper limit of what is achievable with conventional WC-Co cemented carbides of similar grain sizes.

In addition to HV10 hardness, indentation fracture toughness estimates were made and are presented in Table 2. Indentation fracture

Table 2
Mechanical properties of WC-Ni measured at room temperature after HT testing.

Sample	Hardness HV10 [kgf/mm^2]	K_{IC} [MPa·m$^{0.5}$]
W2Ni	2210 ± 34	7.0 ± 0.2
W6Ni	2040 ± 23	8.0 ± 0.1
W14Ni	1588 ± 8	11.0 ± 0.3

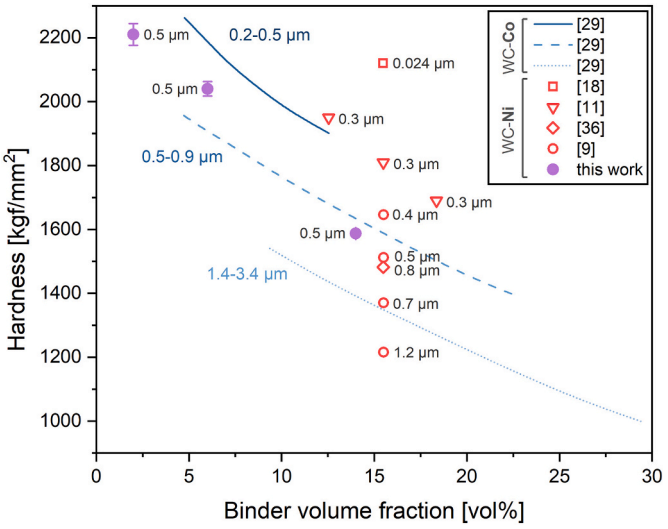

Fig. 10. HV30 and HV10 hardness of cemented carbides produced from WC-Ni [9,11,18,36] and WC-Co [29] against binder content and their average grain size.

toughness is known to suffer substantial errors compared to conventional fracture toughness measurements [32–35]. Therefore, it is not appropriate to compare them to literature values that are obtained using conventional testing methods. However, a positive correlation between Ni content and indentation fracture toughness was seen, consistent with the literature [29]. The small WC grain size and low Ni binder contents prevent high toughness values; nevertheless, the materials possess sufficient resilience to sustain crack growth for low impact applications.

4. Conclusions

A novel processing route for WC-Ni cemented carbides with binder contents between 2 vol% and 14 vol% was investigated regarding sintering behaviour and properties of the resulting cemented carbides. The approach involved the synthesis of Ni coated WC powders by deposition of well-dispersed metallic Ni nano-dots on WC particles using a solution-based route. The powders were consolidated using spark plasma sintering (SPS). The WC-Ni powders exhibited good sinterability with sintering start temperatures between 800 °C and 900 °C. Relative densities of 99 % were achieved without severe WC grain growth when using a heating rate of 100 °C/min. After sintering, Ni redistribution close to the surface and the formation of small amounts of η-phase in some of the compositions were observed.

In the low binder content samples, the room temperature hardness was exceptionally high compared to conventional WC-Co cemented carbides while maintaining sufficient toughness for low impact applications. This demonstrates the suitability of this processing route, especially for low binder content compositions. High-temperature hardness exhibited a gradual decrease without abrupt changes up to 700 °C. Overall, our findings provide insights into the applicability of solution-based powder coating in combination with SPS for producing high-performance WC-Ni cemented carbides with low binder contents.

CRediT authorship contribution statement

Paul H. Gruber: Methodology, Validation, Formal analysis, Investigation, Data curation, Visualization, Writing - original draft, Writing - review & editing. **Sarmad Naim Katea:** Methodology, Investigation, Writing - review & editing. **Gunnar Westin:** Conceptualization, Methodology, Project administration, Funding acquisition, Validation, Supervision, Resources, Writing - review & editing. **Farid Akhtar:** Conceptualization, Supervision, Project administration, Funding acquisition, Resources, Writing - review & editing.

Declaration of Competing Interest

The authors of the manuscript certify that they have NO affiliations with or involvement in any organization or entity with any financial interest (such as honoraria; educational grants; participation in speakers' bureaus; membership, employment, consultancies, stock ownership, or other equity interest; and expert testimony or patent-licensing arrangements), or non-financial interest (such as personal or professional relationships, affiliations, knowledge or beliefs) in the subject matter or materials discussed in this manuscript.

Data availability

Data will be made available on request.

Acknowledgements

This work was performed in the SUNRISE Centre with financial support from the Swedish Foundation for Strategic Research (SSF) under Grant No. ARC19-0043. The authors are grateful for the support. Parts of this work were also funded by the Austrian COMET Program (project K2 InTribology, no. 872176) and carried out at the "Excellence Centre of Tribology" AC2T research GmbH. The authors also thank LUMIA (Luleå Material Imaging and Analysis) for providing instruments for SEM and XRD characterisation and the MSL facilities at the Ångström laboratory, Uppsala University for providing a SEM for studies of powders.

During the preparation of this work, the authors used DeepL Write and ChatGPT to improve readability and restructure some sentences. After using those tools, the authors reviewed and edited the content as needed and took full responsibility for the publication's content.

Appendix A. Supplementary data

Supplementary data to this article can be found online at https://doi.org/10.1016/j.ijrmhm.2023.106375.

References

[1] K. Schröter, Gesinterte harte Metalllegierungen und Verfahren zu ihrer Herstellung, DE Patent C. 420689 (1923) 30.
[2] R. Steinlechner, R. de Oro Calderon, T. Koch, P. Linhardt, W.D. Schubert, A study on WC-Ni cemented carbides: constitution, alloy compositions and properties, including corrosion behaviour, Int. J. Refract. Met. Hard Mater. 103 (2022), https://doi.org/10.1016/j.ijrmhm.2021.105750.
[3] W.M. Daoush, K.H. Lee, H.S. Park, S.H. Hong, Effect of liquid phase composition on the microstructure and properties of (W,Ti)C cemented carbide cutting tools, Int. J. Refract. Met. Hard Mater. 27 (2009) 83–89, https://doi.org/10.1016/j.ijrmhm.2008.04.003.
[4] J. Yang, X. Miao, X. Wang, F. Yang, Influence of Mn additions on the microstructure and magnetic properties of FeNiCr/60% WC composite coating produced by laser cladding, Int. J. Refract. Met. Hard Mater. 46 (2014) 58–64, https://doi.org/10.1016/j.ijrmhm.2014.05.010.
[5] V.A. Tracey, Nickel in Hardmetals, Int. J. Refract. Met. Hard Mater. 11 (1992) 137–149.
[6] H. Suzuki, K. Hayashi, T. Yamamoto, N. Chujo, Relations between some properties of sintered WC-10%Ni alloy and its binder phase composition, J. Jpn. Soc. Powder Powder Metal. 13 (1966) 290–295, https://doi.org/10.2497/jjspm.13.290.
[7] S. Takeda, Science reports of the Tohoku Imperial University, Honda Anniv. (1936) 864–881.
[8] L. Suk-Joong, Kang, Sintering: Densification, Grain Growth and Microstructure, Elsevier Science, 2004.
[9] H. Suzuki, K. Hayashi, O. Terada, Mechanical properties of micro-grained WC-Ni cemented carbide, J. Jpn. Soc. Powder Powder Metal. 42 (1995) 1345–1349, https://doi.org/10.2497/jjspm.42.1345.
[10] H. Rong, Z. Peng, X. Ren, Y. Peng, C. Wang, Z. Fu, L. Qi, H. Miao, Ultrafine WC-Ni cemented carbides fabricated by spark plasma sintering, Mater. Sci. Eng. A 532 (2012) 543–547, https://doi.org/10.1016/j.msea.2011.10.119.
[11] H.C. Kim, I.J. Shon, J.K. Yoon, J.M. Doh, Z.A. Munir, Rapid sintering of ultrafine WC-Ni cermets, Int. J. Refract. Met. Hard Mater. 24 (2006) 427–431, https://doi.org/10.1016/j.ijrmhm.2005.07.002.
[12] Å. Ekstrand, G. Westin, M. Nygren, Homogeneous WC-Co-cemented carbides from a cobalt-coated WC powder produced by a novel solution-chemical route, J. Am.

Ceram. Soc. 90 (2007) 3449–3454, https://doi.org/10.1111/j.1551-2916.2007.01948.x.
[13] S. Naim Katea, C.W. Tai, P.O. Larsson, H. Vidarsson, G. Westin, Nickel dot coating of NbC powder by solution processing, Open Ceram. 4 (2020), https://doi.org/10.1016/j.oceram.2020.100043.
[14] Å. Ekstrand, G. Westin, Highly homogeneous WC-Ni/Co composites produced from WC-powder coated with a solution chemical route, in: 10th Int Ceram Congr 2002 Proc, 2002, p. 489.
[15] Å. Ekstrand, K. Jansson, G. Westin, Solution Synthesis of Nano-Phase Nickel as Film and Porous Electrode, 2000.
[16] Å. Ekstrand, K. Jansson, G. Westin, A solution synthetic route to nanophase cobalt film and sponge, Chem. Mater. 17 (2005) 199–205, https://doi.org/10.1021/cm0494610.
[17] C.M. Fernandes, A.M.R. Senos, M.T. Vieira, Control of eta carbide formation in tungsten carbide powders sputter-coated with (Fe/Ni/Cr), Int. J. Refract. Met. Hard Mater. 25 (2007) 310–317, https://doi.org/10.1016/j.ijrmhm.2006.07.004.
[18] M.J.S. Lima, F.E.S. Silva, H.D. Lima, M.V.M. Souto, A.G.F. Oliveira, R. A. Raimundo, C.P. Souza, U.U. Gomes, Spark plasma sintering of nanostructured powder composites (WC–Ni) prepared by carboreduction reaction, Mater. Chem. Phys. 254 (2020), https://doi.org/10.1016/j.matchemphys.2020.123439.
[19] R.M. Genga, Microstructure and Properties of Selectred WC-Cemented Carbides Manufactured by SPS Method, Johannesburg, 2014.
[20] M. Tokita, Progress of spark plasma sintering (SPS) method, systems, ceramics applications and industrialization, Ceramics. 4 (2021) 160–198, https://doi.org/10.3390/ceramics4020014.
[21] H. Engqvist, B. Uhrenius, Determination of the average grain size of cemented carbides, Int. J. Refract. Met. Hard Mater. 21 (2003) 31–35, https://doi.org/10.1016/S0263-4368(03)00005-2.
[22] M. Varga, M. Flasch, E. Badisch, Introduction of a novel tribometer especially designed for scratch, adhesion and hardness investigation up to 1000°C, in: Proceedings of the Institution of Mechanical Engineers, Part J: J Eng Tribol, SAGE Publications Ltd, 2017, pp. 469–478, https://doi.org/10.1177/1350650115592918.
[23] B. Roebuck, E. Bennett, L. Lay, R. Morrell, Measurement Good Practice Guide No. 9: Palmqvist Toughness for Hard and Brittle Materials, Teddington, Middlesex, UK, 1998.
[24] V.K. Portnoi, A.V. Leonov, S.N. Mudretsova, S.A. Fedotov, Formation of nickel carbide in the course of deformation treatment of Ni-C mixtures, Phys. Met. Metallogr. 109 (2010) 153–161, https://doi.org/10.1134/S0031918X10020079.
[25] C. Suryanarayana, M.G. Norton, X-Ray Diffraction, Springer US, Boston, MA, 1998, https://doi.org/10.1007/978-1-4899-0148-4.
[26] E. Toulkeridou, J. Kioseoglou, P. Grammatikopoulos, On the melting point depression, coalescence, and chemical ordering of bimetallic nanoparticles: the miscible Ni–Pt system, Nanoscale Adv. 4 (2022) 4819–4828, https://doi.org/10.1039/d2na00418f.
[27] J.L. Hay, G.M. Pharr, ASM Handbook, Volume 3: Alloy Phase Diagrams, 2000.
[28] H.R. De Macedo, A.G.P. Da Silva, D.M.A. De Melo, The spreading of cobalt, nickel and iron on tungsten carbide and the first stage of hard metal sintering, Mater. Lett. 57 (2003) 3924–3932, https://doi.org/10.1016/S0167-577X(03)00242-8.
[29] J. García, V. Collado Ciprés, A. Blomqvist, B. Kaplan, Cemented carbide microstructures: a review, Int. J. Refract. Met. Hard Mater. 80 (2019) 40–68, https://doi.org/10.1016/j.ijrmhm.2018.12.004.
[30] I. Konyashin, B. Ries, F. Lachmann, A.T. Fry, Gradient WC-co hardmetals: theory and practice, Int. J. Refract. Met. Hard Mater. 36 (2013) 10–21, https://doi.org/10.1016/j.ijrmhm.2011.12.010.
[31] R. Juškenas, I. Valsiunas, V. Pakštas, R. Giraitis, On the state of W in electrodeposited Ni-W alloys, Electrochim. Acta 54 (2009) 2616–2620, https://doi.org/10.1016/j.electacta.2008.10.060.
[32] G.D. Quinn, Fracture Toughness of Ceramics by the Vickers Indentation Crack Length Method: A Critical Review, 2008, pp. 45–62, https://doi.org/10.1002/9780470291313.ch5.
[33] N. Ingelstrom, H. Nordberg, The Fracture Toughness of Cemented Tungsten Carbides, Pcrgamon Press, 1974.
[34] I.M. Ogilvy, C.M. Perrott, J.W. Suiter, On the Indentation Fracture of Cemented Carbide Part 1 - Survey of Operative Fracture Modes, Elsevier Sequoia S.A, 1977.
[35] Y. Torres, D. Casellas, M. Anglada, L. Llanes, Fracture Toughness Evaluation of Hardmetals: In Uence of Testing Procedure. www.elsevier.nl/locate/ijrmhm, 2023.
[36] R.M. Genga, P. Rokebrand, L.A. Cornish, N. Nelwalani, G. Brandt, N. Kelling, M. Woydt, A.J. van Vuuren, C. Polese, High-temperature sliding wear, elastic modulus and transverse rupture strength of Ni bonded NbC and WC cermets, Int. J. Refract. Met. Hard Mater. 87 (2020), https://doi.org/10.1016/j.ijrmhm.2019.105143.